Journal of Fluids and Structures 17 (2003) 345–350

JOURNAL OF FLUIDS AND STRUCTURES

www.elsevier.nl/locate/jnlabr/yjfls

Some vortex-shedding characteristics of the staggered configuration of circular cylinders

D. Sumner*, M.D. Richards

Department of Mechanical Engineering, University of Saskatchewan, 57 Campus Drive, Saskatoon, Saskatchewan, Canada S7N 5A9

Received 14 November 2000; received in revised form 6 June 2002

Abstract

A pair of circular cylinders of equal diameter arranged in the staggered configuration was tested in the subcritical Reynolds number regime at centre-to-centre pitch ratios of $P/D = 2.0$ and 2.5. For each pitch ratio, the incidence angle was varied in small steps in the range $\alpha = 0-90^\circ$. Vortex-shedding frequency measurements were made behind the upstream and downstream cylinders as the incidence angle, α, was varied. At small incidence angles, $2^\circ < \alpha < 15^\circ$, the Strouhal number data were unreliable, since the peaks in the power spectra were either absent or broad banded. In this same range of incidence angle, the downstream cylinder experiences a maximum inward-directed lift force and a minimum drag force. The results indicate that the flow mechanisms responsible for the changes in the aerodynamic forces have an important influence on the vortex-shedding activity also.

1. Introduction

Groups of circular cylinders immersed in cross-flow arise in a number of engineering applications. Some of these include the designs for heat exchangers, cooling systems for nuclear power plants, offshore structures, buildings, chimneys, and power transmission lines. In many of these cases, vortex shedding may be responsible for flow-induced vibrations and noise. The most general configuration of two circular cylinders, of equal diameter, D, immersed in a steady mean cross-flow of velocity, U, is known as the staggered arrangement; see Fig. 1(a). Here, the cylinders are spaced at a centre-to-centre distance, P, and at an angle, α, to the oncoming mean flow. The behaviour of the flow is known to be highly sensitive to the combination of the nondimensional pitch ratio, P/D, and the incidence angle, α.

The complexity of the flow around the staggered configuration has been revealed in a number of experimental studies. Recent flow visualisation and PIV experiments by Sumner et al. (2000) conducted within the low subcritical regime ($\mathrm{Re} = 850 - 1900$, based on the cylinder diameter) have identified up to nine distinct flow patterns. These patterns incorporate various aspects of shear layer reattachment (SLR), alternate vortex shedding from one or both cylinders, vortex splitting, pairing and enveloping, synchronised vortex shedding, and vortex impingement. A similar study by Gu and Sun (1999), which was conducted at very high subcritical Reynolds numbers ($\mathrm{Re} = 2.2 \times 10^5 - 3.3 \times 10^5$), identified three main flow patterns for the staggered configuration. Despite the difference in Reynolds number between the studies, many of the flow features identified by Gu and Sun (1999) and Sumner et al. (2000) are consistent, particularly at small and intermediate P/D and α.

Studies that have measured the aerodynamic forces on the cylinders have shown a number of interesting features, particularly for the downstream cylinder (Zdravkovich and Pridden, 1977; Gu and Sun, 1999). Noteworthy is the existence of an "inner" lift peak at small P/D and α. Here, the mean inward-directed lift force on the downstream

*Corresponding author.
E-mail address: david.sumner@usask.ca (D. Sumner).

0889-9746/03/$ - see front matter
PII: S0889-9746(02)00145-7

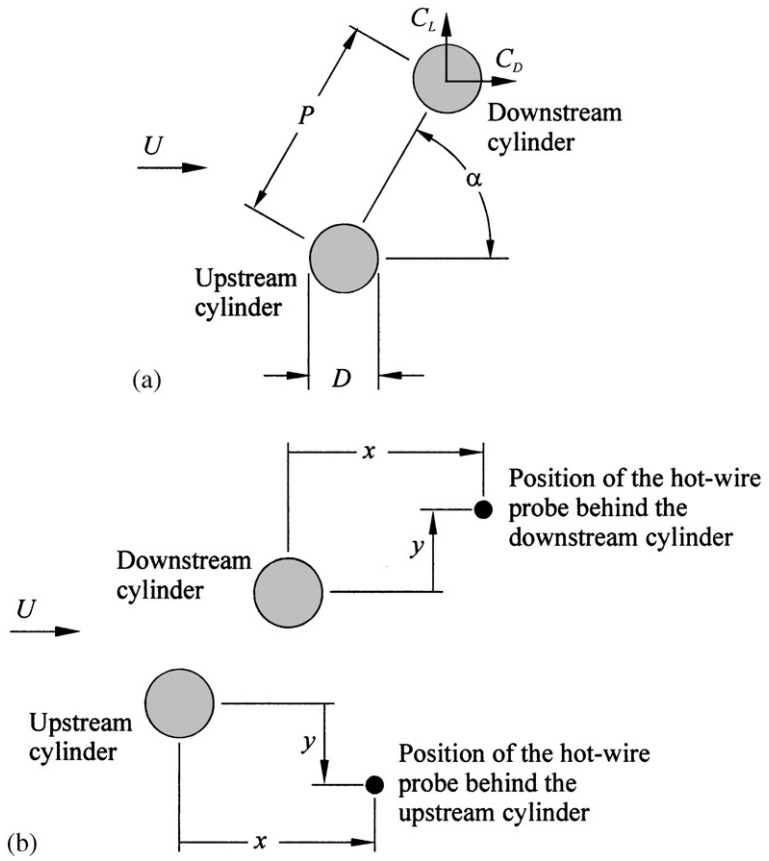

Fig. 1. (a) Nomenclature for the staggered configuration of two circular cylinders of equal diameter, immersed in a steady mean cross-flow. Included is the force convention for the downstream cylinder. (b) The position of the hot-wire probe relative to the upstream and downstream cylinders.

cylinder reaches a maximum. The maximum lift is highly sensitive to changes in P/D and α, and it abruptly disappears as the incidence tends to $\alpha = 0^\circ$. Also, the inner lift peak coincides with a minimum drag force on the downstream cylinder. Based on the results of Gu and Sun (1999) and Sumner et al. (2000), this behaviour of the aerodynamic forces on the downstream cylinder is thought to be highly dependent on the tendency towards SLR on the downstream cylinder, and its sudden appearance or disappearance as P/D and α are varied. The mean aerodynamic forces are expressed in dimensionless form as lift and drag force coefficients, C_L and C_D, respectively. The directions of the two force components on the downstream cylinder are shown in Fig. 1(a).

The same flow conditions that contribute to the inner lift peak and the minimum drag ought to have a similar influence on the vortex-shedding frequency measurements. The vortex-shedding frequency, f, is expressed in nondimensional form as the Strouhal number, St $(= fD/U)$. Depending on the flow pattern more than one Strouhal number may be measured for the staggered configuration (Kiya et al., 1980; Sumner et al. 2000). Because of the limited angular resolution of the published St data, however, the characteristics noticed for the aerodynamic forces have not been reported for the St measurements. In this study, the behaviour of the vortex-shedding frequency measurements is examined in more detail.

2. Experimental approach

Experiments were conducted in a low-speed, closed-return wind tunnel, with a test-section of 0.91 m (height) × 1.13 m (width) × 1.96 m (length). The longitudinal freestream turbulence intensity was no greater than 0.6% and the freestream

nonuniformity in the central portion of the test-section, outside the test-section-wall boundary layers, was no greater than 0.5%. Freestream conditions were monitored with a Pitot-static probe and a pair of pressure transducers. Data were acquired with a National Instruments AT-MIO-64F-5 multifunction board and LabVIEW.

Two smooth circular cylinders, with $D = 32.1$ mm, an aspect ratio of 24, and a solid blockage ratio of 2.8% per cylinder, were placed between circular end-plates. No wall interference corrections were made. Data are presented for two dimensionless pitch ratios, $P/D = 2.0$ and 2.5. For each P/D, the incidence was varied in small increments from $\alpha = 0$ to 90°. The uncertainty in the angular position was estimated at $\pm 0.25°$. Experiments were conducted at $\mathrm{Re} = 3.2 \times 10^4 - 7.0 \times 10^4$. To measure the aerodynamic forces, the downstream cylinder was mounted on a six-component force balance. The uncertainty in the aerodynamic force coefficients ranged from $\pm 4\%$ at $\mathrm{Re} = 3.2 \times 10^4$ to $\pm 1\%$ at $\mathrm{Re} = 7.0 \times 10^4$. Vortex-shedding frequencies were acquired with a TSI 1210-T1.5 single-component hot-wire probe, an IFA-100 anemometer, a National Instruments PCI-6024E data-acquisition board, and the Virtual Bench Digital Signal Analyser. The measurement uncertainty in St ranged from $\pm 6\%$ at $\mathrm{Re} = 3.2 \times 10^4$ to $\pm 3\%$ at $\mathrm{Re} = 7.0 \times 10^4$. Since the detection of a St number for the upstream cylinder is highly sensitive to the measurement location (Kiya et al., 1980; Sumner et al., 2000), the hot-wire probe was located at various positions to ensure the reliability and repeatability of the power spectra. The probe was typically positioned at $x/D = 3.0$ and $y/D = 1.0$ from the downstream cylinder, and at $x/D = 3.0$ and $y/D = 1.0$ from the upstream cylinder (Fig. 1(b)).

3. Results and discussion

Measurements of the aerodynamic forces on the downstream cylinder (Fig. 2) clearly show the inner lift peak and the drag minimum at $\alpha = 9°$, for both $P/D = 2.0$ and 2.5. For $\alpha < 9°$, the lift force suddenly disappears and there are some further changes in the drag force. For $\alpha > 9°$, the lift force more gradually approaches zero-lift and the drag force increases. The force data were independent of Reynolds number for $\mathrm{Re} = 3.2 \times 10^4 - 7.0 \times 10^4$.

The St number data (Fig. 2), measured behind the upstream and downstream cylinders, also were independent of Reynolds number over the range studied. For most incidence angles, $15° < \alpha < 90°$, two distinct St numbers were measured, which was consistent with published data (Kiya et al., 1980; Sumner et al., 2000). The power spectra (Fig. 3) show that the higher Strouhal number corresponds to vortex shedding from the upstream cylinder and the lower St number to vortex shedding from the downstream cylinder. As the tandem configuration is approached, $\alpha = 0°$, the cylinders are known to behave in a similar fashion to a single bluff-body, and only a single vortex street is observed (Sumner et al., 2000). Consequently, only a single St number is measured. As the side-by-side configuration is approached, $\alpha = 90°$, the cylinders become increasingly independent of one another. At $\alpha = 90°$, each cylinder sheds vortices at the same frequency, and the two St numbers have converged to the value for a single, isolated circular cylinder, $St \approx 0.2$, for both $P/D = 2.0$ and 2.5.

At small incidence angles, $2° < \alpha < 15°$, the St number data were unreliable, since the peaks in the power spectra were either absent or broad banded; the shaded regions in Fig. 2 denote this result. The nonexistent or broad-banded peaks are detected at the same α values associated with the maximum inward-directed lift force, and minimum drag force, experienced by the downstream cylinder (Zdravkovich and Pridden, 1977; Gu and Sun, 1999), also shown in Fig. 2. Other researchers have not extensively reported this result, because only a limited number of incidence-angle positions have typically been examined, and few studies of the staggered configuration have reported measurements of both the aerodynamic forces and the vortex-shedding frequencies together.

Selected power spectra are presented in Fig. 3, for $P/D = 2.0$ and 2.5. As shown, for $2° < \alpha < 15°$, the peaks in the power spectra behind both cylinders are either absent or broad banded. For $P/D = 2.0$ (Fig. 3(a)), for both cylinders, broad-banded spectral peaks are seen at $\alpha = 4°$ and the peaks are absent at $\alpha = 8°$ and 10°. For $P/D = 2.5$ (Fig. 3(b)), strong broad-banded peaks are observed for both cylinders at $\alpha = 4°$, while weaker broad-banded peaks can be discerned for the downstream cylinder at $\alpha = 6°$, 8° and 10°. For the upstream cylinder, peaks are absent from the power spectra at $\alpha = 6°$, 8° and 10°.

As with the aerodynamic forces, the origins of the absent and broad-banded peaks in the power spectra are associated with the marked flow pattern changes at small α (Gu and Sun, 1999; Sumner et al., 2000); the various flow pattern boundaries and designations are indicated in Fig. 2. For $\alpha < 15°$, the flow pattern is highly sensitive to the behaviour of the inner shear layer from the upstream cylinder. This shear layer may reattach onto the outside of the downstream cylinder, patterns $\mathrm{I_B}$ and SLR denoted in Fig. 2. Alternatively, the shear layer may be deflected through the gap between the cylinders and attach onto the inside leading face of the downstream cylinder, patterns $\mathrm{II_B}$ and IS denoted in Fig. 2. In each of these cases, patterns $\mathrm{I_B}$, SLR, $\mathrm{II_B}$, and IS, periodic vortex shedding from the upstream cylinder is suppressed. Vortex shedding from the downstream cylinder is also influenced, for $2° < \alpha < 15°$, since the peaks in the power spectra for the downstream cylinder are mostly absent or broad banded also; see Fig. 3.

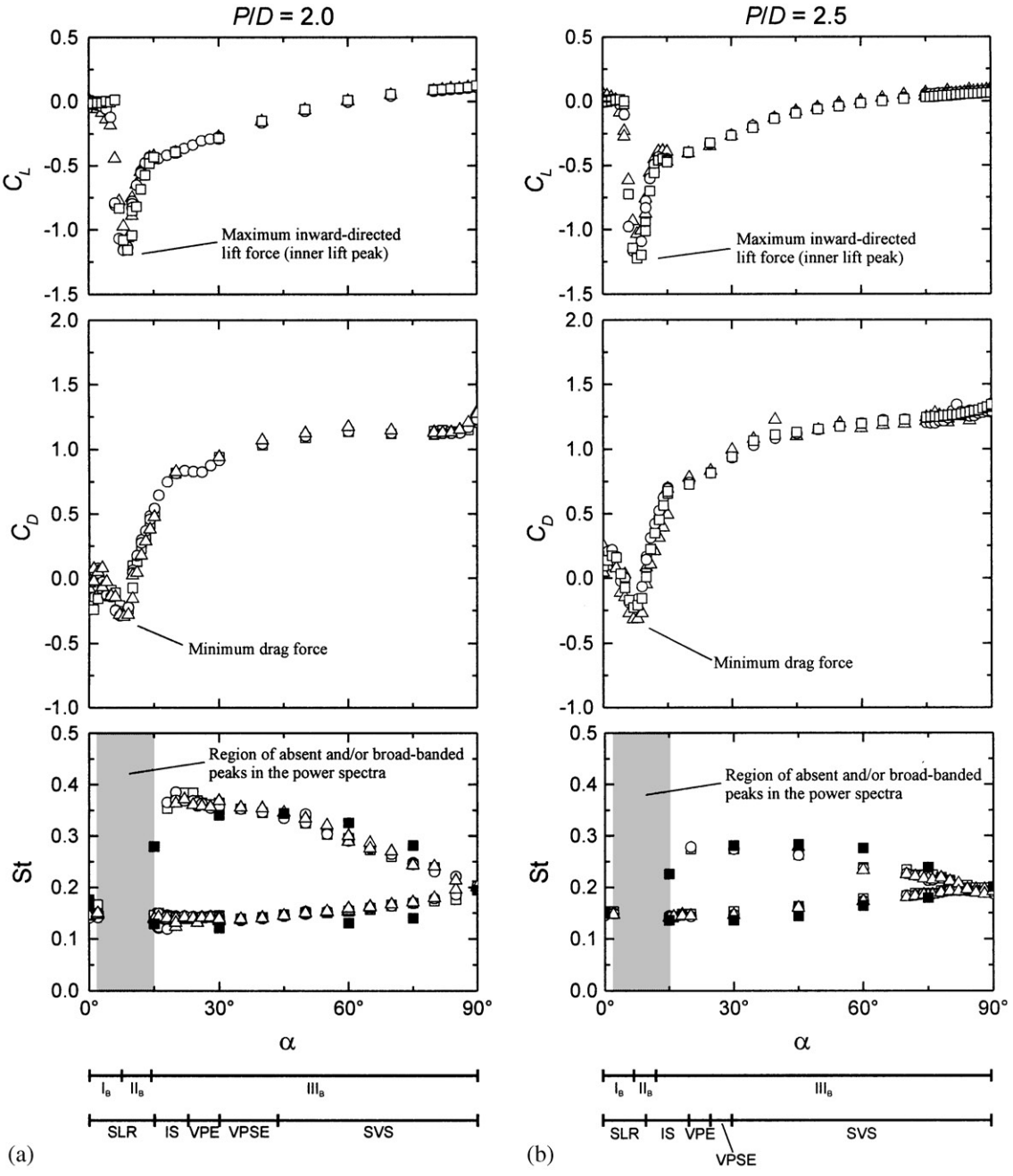

Fig. 2. Mean aerodynamic forces and *St* number data, □, $Re = 3.2 \times 10^4$; ○, $Re = 5.6 \times 10^4$; △, $Re = 7.0 \times 10^4$; ■, Kiya et al. (1980), $Re = 1.6 \times 10^4$: (a) $P/D = 2.0$ and (b) $P/D = 2.5$. Flow pattern boundaries of Gu and Sun (1999), $Re = 2.2 \times 10^5 - 3.3 \times 10^5$: Patterns I_B, II_B and III_B. Flow pattern boundaries of Sumner et al. (2000), $Re = 850 - 1900$ SLR (shear layer reattachment), IS (induced separation), VPE (vortex pairing and enveloping), VPSE (vortex pairing, splitting and enveloping), and SVS (synchronized vortex shedding).

When α is increased, $\alpha > 15°$, the inner shear layer from the upstream cylinder no longer interacts directly with the downstream cylinder. Instead, this shear layer becomes part of the alternate vortex-shedding process behind the upstream cylinder, which is observed for patterns III_B, VPE, VPSE, and SVS denoted in Fig. 2. The peaks then reappear in the power spectra for both cylinders; see Fig. 3. Further details on the flow patterns may be found in Gu and Sun (1999) and Sumner et al. (2000).

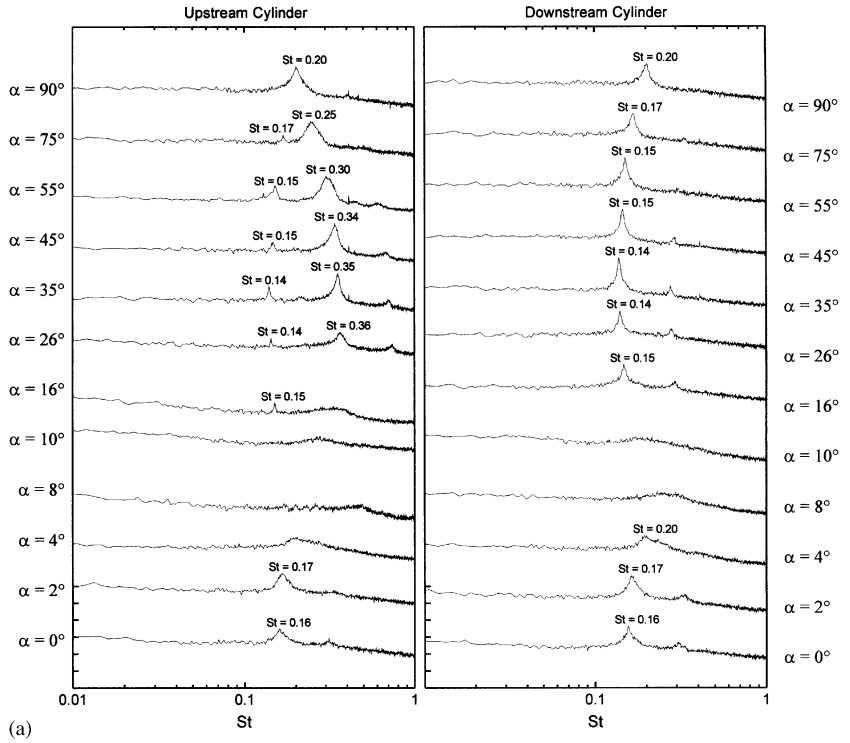

(a)

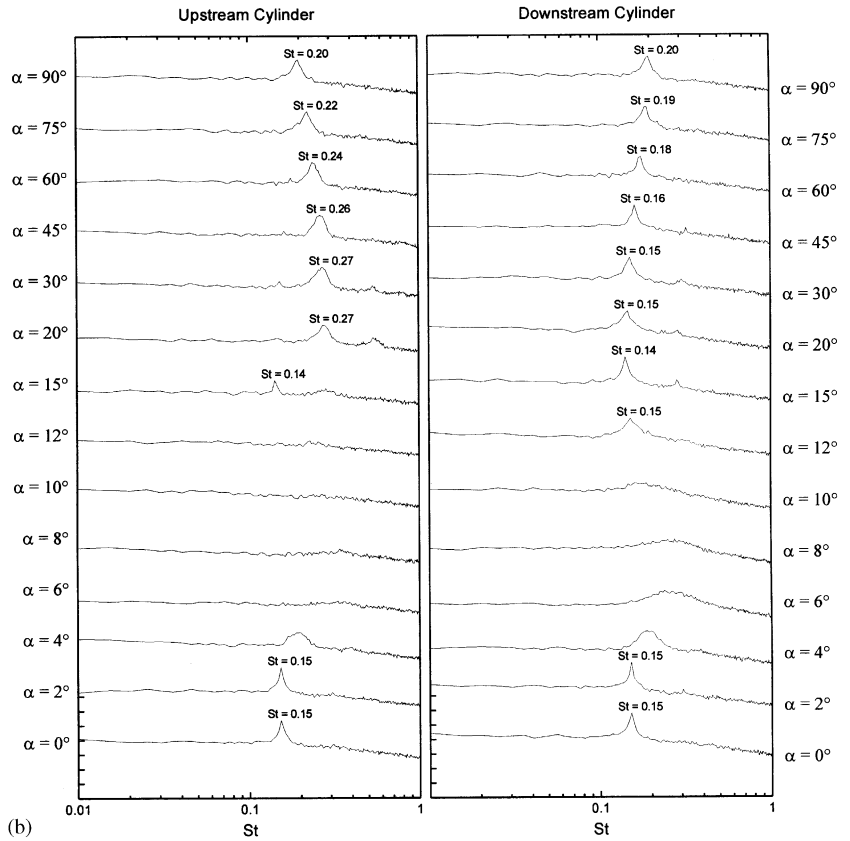

(b)

Fig. 3. Selected power spectra, as a function of incidence angle, measured behind the upstream and downstream cylinders, $\mathrm{Re} = 3.2 \times 10^4$: (a) $P/D = 2.0$ and (b) $P/D = 2.5$. Measurement positions vary for each spectrum. Each spectrum represents 250 averages. The vertical scale is arbitrary, but the same scale is used for each spectrum.

4. Conclusions

The vortex-shedding frequencies for a staggered configuration of two circular cylinders, with $P/D = 2.0$ and 2.5, were measured within the subcritical Reynolds number regime. The existence of broad-banded power spectra and the absence of sharply defined spectral peaks, from $2^\circ < \alpha < 15^\circ$, coincides with the inner lift force maximum and a region of minimum drag force for the downstream cylinder reported by other researchers. The absence of reliable Strouhal (St) number data in this incidence-angle range is consistent with the marked changes in the vortex-shedding activity and the flow pattern at small α, and with the sensitivity of the aerodynamic forces on the downstream cylinder. This sudden appearance or disappearance of periodic vortex-shedding activity at small incidence angles, which may occur if the mean flow direction varies, is problematic for the reliable prediction of vortex-induced vibrations in staggered cylinder configurations. Further studies are now underway to discover the extent of the unreliable St data at other P/D ratios, and to clarify the relationships between the flow pattern boundaries, aerodynamic forces, and the Reynolds number.

Acknowledgements

The support of the Natural Sciences and Engineering Research Council (NSERC) of Canada is gratefully acknowledged. The assistance of D. Deutscher and J.L. Heseltine is appreciated.

References

Gu, Z.F., Sun, T.F., 1999. On interference between two circular cylinders in staggered arrangement at high subcritical Reynolds numbers. Journal of Wind Engineering and Industrial Aerodynamics 80, 287–309.

Kiya, M., Arie, M., Tamura, H., Mori, H., 1980. Vortex shedding from two circular cylinders in staggered arrangement. ASME Journal of Fluids Engineering 102, 166–173.

Sumner, D., Price, S.J., Païdoussis, M.P., 2000. Flow-pattern identification for two staggered circular cylinders in cross-flow. Journal of Fluid Mechanics 411, 263–303.

Zdravkovich, M.M., Pridden, D.L., 1977. Interference between two circular cylinders; series of unexpected discontinuities. Journal of Industrial Aerodynamics 2, 255–270.